



HAL
open science

Fully smoothed ℓ_1 -TV models: Bounds for the minimizers and parameter choice

F. Baus, Mila Nikolova, Gabriele Steidl

► **To cite this version:**

F. Baus, Mila Nikolova, Gabriele Steidl. Fully smoothed ℓ_1 -TV models: Bounds for the minimizers and parameter choice. *Journal of Mathematical Imaging and Vision*, 2013, 10.1007/s10851-013-0420-0 . hal-00722743v3

HAL Id: hal-00722743

<https://hal.science/hal-00722743v3>

Submitted on 4 Feb 2013

HAL is a multi-disciplinary open access archive for the deposit and dissemination of scientific research documents, whether they are published or not. The documents may come from teaching and research institutions in France or abroad, or from public or private research centers.

L'archive ouverte pluridisciplinaire **HAL**, est destinée au dépôt et à la diffusion de documents scientifiques de niveau recherche, publiés ou non, émanant des établissements d'enseignement et de recherche français ou étrangers, des laboratoires publics ou privés.

Fully smoothed ℓ_1 -TV models: Bounds for the minimizers and parameter choice

F. Baus, M. Nikolova, and G. Steidl

February 4, 2013

Abstract

We consider a class of convex functionals that can be seen as \mathcal{C}^1 smooth approximations of the ℓ_1 -TV model. The minimizers of such functionals were shown to exhibit a qualitatively different behavior compared to the nonsmooth ℓ_1 -TV model [11]. Here we focus on the way the parameters involved in these functionals determine the features of the minimizers \hat{u} . We give explicit relationships between the minimizers and these parameters.

Given an input digital image f , we prove that the error $\|\hat{u} - f\|_\infty$ obeys $b - \varepsilon \leq \|\hat{u} - f\|_\infty \leq b$ where b is a constant independent of the input image. Further we can set the parameters so that $\varepsilon > 0$ is arbitrarily close to zero. More precisely, we exhibit explicit formulae relating the model parameters, the input image f and the values b and ε . Conversely, we can fix the parameter values so that the error $\|\hat{u} - f\|_\infty$ meets some prescribed b, ε . All theoretical results are confirmed using numerical tests on natural digital images of different sizes with disparate content and quality.

Keywords Parameter estimation for smoothed ℓ_1 -TV model; Histogram specification; Quantisation noise; ℓ_∞ error; Convex optimization

1 Introduction

In [11] a variational method using \mathcal{C}^2 smoothed ℓ_1 -TV functionals were proposed. The goal was to process digital (quantized) images so that the obtained minimizer is quite close to the input digital image but its pixels are real-valued and can be ordered in a strict way. Indeed, the obtained minimizers were shown to enable faithful *exact histogram specification* outperforming the state-of-the-art methods [7, 12]. The intuition behind these functionals was that their minimizer can up to some degree remove some quantization noise and in this way yield an ordering of the pixels close to the unknown original real-valued image. Such an effect can be observed in Fig. 1 where a synthetic real-valued image is quantized and then restored using the proposed variational method. The *nonsmooth* L_1 -TV model was originally studied in [5]. The main feature of its minimizers is that they contain parts that are equal to the data image and parts that are constant (living in a vanishing component of the TV term). Even though the model modification proposed in [11] might seem trivial, the minimizers of these \mathcal{C}^2 smoothed ℓ_1 -TV functionals exhibit a *qualitatively* different behavior. Unlike the L_1 -TV (ℓ_1 -TV) minimizers, it was shown in [11] that the minimizers of the \mathcal{C}^2 smoothed ℓ_1 -TV functionals generically do not have pixels equal to those of the data image and there are no equally valued pixels. Some of the authors of [11] observed that once the parameters of the model were fixed, for all kind of real-world digital images f , the residual error obeyed $\|\hat{u} - f\|_\infty = b$ where the constant b typically met $b < 0.5$. For this reason, they qualified this variational approach as *detail preserving*. Therefore we were interested in monitoring the error $\|\hat{u} - f\|_\infty$.

In this paper we consider a wider class of \mathcal{C}^1 smoothed ℓ_1 -TV functionals involving also ℓ_2 data fidelity terms. We give explicit relationships between the minimizers and the parameters tuning the model. The observation that $\|\hat{u} - f\|_\infty = b$, up to a small difference, is independent of

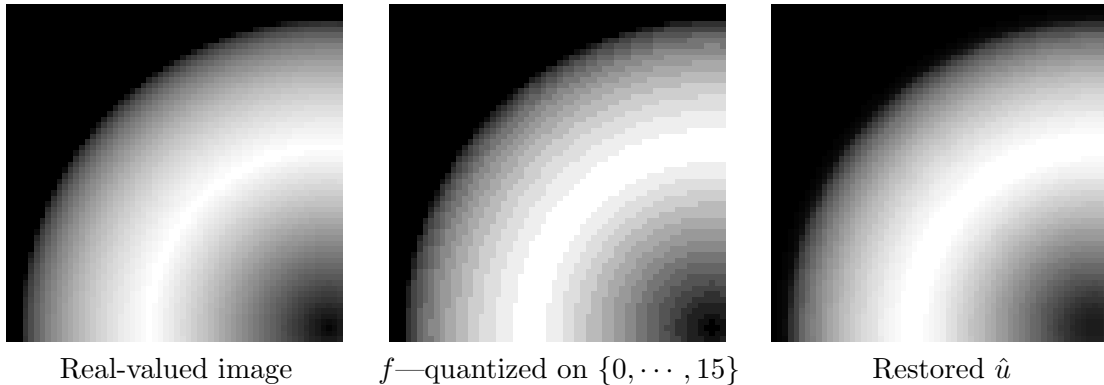


Figure 1: The restored image is obtained by minimizing $J(\cdot, f)$ of the form (1) where $\psi(t) = \sqrt{t^2 + \alpha_1}$ and $\varphi(t) = \sqrt{t^2 + \alpha_2}$ for $\mathcal{N}8$.

the input image, is confirmed theoretically. Clear indications on the role of the parameter setting and the lower and upper bounds of $\|\hat{u} - f\|_\infty$ enable us to give restrictions on the parameter selection. All theoretical results are confirmed using numerical tests on a set of digital images of different sizes with disparate content and quality.

In spite of the progress in nonsmooth convex optimization [4], smooth approximations of nonsmooth objectives still remain a common approach in optimization [2]. Our results can help to design smooth approximations of ℓ_1/ℓ_2 -TV functionals in a proper way.

The outline of this paper is as follows: In the next Section 2 we describe the variational model. Then, in Section 3 we estimate the ℓ_∞ -error between the input image f and the minimizer of the functional. Section 4 provides explicit parameter estimates for the model. In Section 5 we give probability estimates for the behavior of neighboring pixels. Numerical tests demonstrate the quality of our estimates in Section 6. Finally, Section 7 finishes with conclusions and perspectives.

2 The Fully Smoothed ℓ_1 -TV Model

We consider $M \times N$ digital images f with gray values in $\{0, \dots, L - 1\}$. Let $n := MN$. To simplify the notation we reorder the image columnwise into a vector of size n and address the pixels by the index set $\mathbb{I}_n := \{1, \dots, n\}$. Further, we denote by $\mathbb{I}_n^{\text{int}} \subset \mathbb{I}_n$ the subset of all inner pixels, i.e., all pixels which are not boundary pixels.

We are interested in the minimizer \hat{u} of a functional of the form

$$J(u, f) := \Psi(u, f) + \beta\Phi(u), \quad \beta > 0 \tag{1}$$

with

$$\begin{aligned} \Psi(u, f) &:= \sum_{i \in \mathbb{I}_n} \psi(u[i] - f[i]), \\ \Phi(u) &:= \sum_{i \in \mathbb{I}_n} \sum_{j \in \mathcal{N}_i} \varphi(\gamma_{i,j}(u[i] - u[j])), \end{aligned}$$

where \mathcal{N}_i is a neighborhood of pixel i , the $\gamma_{i,j} > 0$ are weighting terms for the distance between neighbors, and the functions ψ and φ depend on a positive parameter, α_1 and α_2 , respectively. To emphasize this dependence we use the notation $\psi(\cdot, \alpha_1)$ and $\varphi(\cdot, \alpha_2)$ when necessary. So $\psi : \mathbb{R} \times (0, +\infty) \rightarrow \mathbb{R}$ and $\varphi : \mathbb{R} \times (0, +\infty) \rightarrow \mathbb{R}$. The functions ψ and φ have to fulfill the properties stated below:

H0 The functions $t \mapsto \psi(t, \alpha_1)$ and $t \mapsto \varphi(t, \alpha_2)$ are continuously differentiable and even.

We denote

$$\psi'(t, \alpha_1) := \frac{d}{dt}\psi(t, \alpha_1) \quad \text{and} \quad \varphi'(t, \alpha_2) := \frac{d}{dt}\varphi(t, \alpha_2) .$$

When it is clear from the context, we write $\psi'(t)$ for $\psi'(t, \alpha_1)$ and $\varphi'(t)$ for $\varphi'(t, \alpha_2)$. By **H0**, $\psi'(t)$ and $\varphi'(t)$ are continuous and odd functions.

These derivative functions have to satisfy certain conditions given next.

H1 ψ $t \mapsto \psi'(t, \alpha_1) : \mathbb{R} \rightarrow (-Y, Y)$, where $Y > 0$, is a strictly increasing function for any fixed $\alpha_1 \in (0, +\infty)$ and maps onto $(-Y, Y)$.

H2 ψ There is a constant $T > 0$ such that for any fixed $t \in (0, T)$, the function $\alpha_1 \mapsto \psi'(t, \alpha_1)$ is strictly decreasing on $(0, +\infty)$.

Here the cases $T = +\infty$ and $Y = +\infty$ are included.

H1 φ $t \mapsto \varphi'(t, \alpha_2)$ is an increasing function for any fixed $\alpha_2 \in (0, +\infty)$ satisfying

$$\lim_{t \rightarrow \infty} \varphi'(t, \alpha_2) = 1.$$

H2 φ For any fixed $t > 0$, the function $\alpha_2 \mapsto \varphi'(t, \alpha_2)$ is continuous and decreasing on $(0, +\infty)$ and

$$\lim_{\alpha_2 \searrow 0} \varphi'(t, \alpha_2) = 1.$$

These properties imply further useful relations which are collected in the following remark.

Remark 1 i) By **H1 ψ** we know that ψ is strictly convex and monotone increasing on $(0, +\infty)$ and by **H1 φ** that φ is convex. Therefore there exists a unique minimizer of (1). This minimizer can be computed, e.g. by using a Weiszfeld-like semi-implicit algorithm, or the nonlinear (pre-conditioned) conjugate gradient method, see [6, 11, 13], among other viable algorithms.

ii) By **H1 ψ** there exists the inverse function $(\psi')^{-1}(\cdot, \alpha_1) : (-Y, Y) \rightarrow \mathbb{R}$, and this function is also odd, continuous and strictly increasing.

Some relevant choices of functions θ obeying all properties **H0**, **H1 ψ** , **H2 ψ** , **H1 φ** and **H2 φ** are given in Table 1. For the latter functions, $t \mapsto \theta'(t, \alpha)$ maps onto $(-1, 1)$, i.e., $Y = 1$ and $T = +\infty$ for any $\alpha > 0$. A typical graph of such a function, its derivative and inverse derivative is depicted in Fig. 2.

	θ	θ'	$(\theta')^{-1}$
$\Theta 1$	$\sqrt{t^2 + \alpha}$	$\frac{t}{\sqrt{t^2 + \alpha}}$	$y\sqrt{\frac{\alpha}{1 - y^2}}$
$\Theta 2$	$ t - \alpha \log\left(1 + \frac{ t }{\alpha}\right)$	$\frac{t}{\alpha + t }$	$\frac{\alpha y}{1 - y }$
$\Theta 3$	$\alpha \log\left(\cosh\left(\frac{t}{\alpha}\right)\right)$	$\tanh\left(\frac{t}{\alpha}\right)$	$\alpha \operatorname{atanh}(y)$

Table 1: Options for functions θ obeying all the assumptions stated above. These functions are nearly affine beyond a neighborhood of zero. The size of the latter neighborhood is controlled by the parameter $\alpha > 0$.

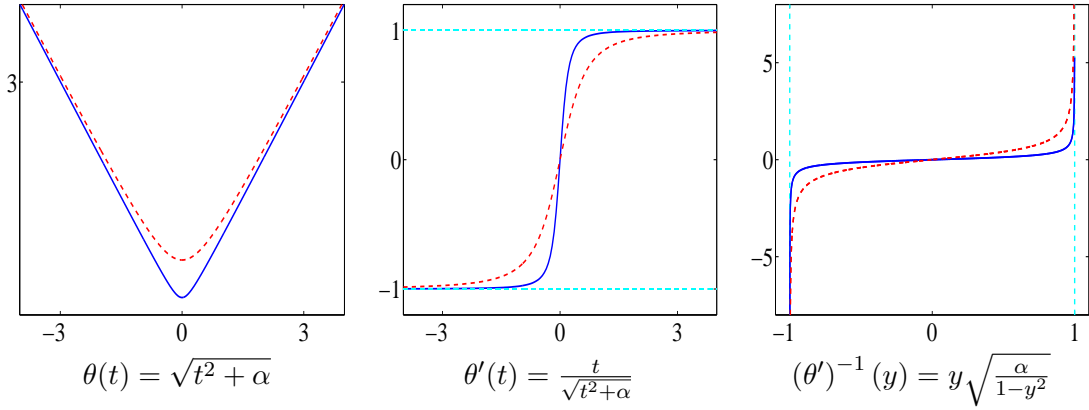


Figure 2: The function $\Theta 1$ in Table 1, where the plots for $\alpha = 0.05$ are in blue solid line and for $\alpha = 0.5$ in red dashed line.

Another choice for ψ fulfilling H0, H1 $^\psi$ and H2 $^\psi$ is the scaled ℓ_p -norm for $p = \alpha_1 + 1$:

$$\psi(t) := \frac{1}{\alpha_1 + 1} |t|^{\alpha_1 + 1} \quad \text{with} \quad \psi'(t) = |t|^{\alpha_1} \text{sign}(t), \quad (\psi')^{-1}(y) = |y|^{\frac{1}{\alpha_1}}, \quad \alpha_1 > 0. \quad (2)$$

Here ψ' maps onto \mathbb{R} so that $Y = +\infty$. Moreover $\alpha_1 \mapsto \psi'(t, \alpha_1)$ is strictly monotone decreasing for $|t| < 1$ hence $T = 1$ in this case. An upper bound for $\|\hat{u} - f\|_\infty$ when $\alpha_1 = 1$ in (2) was derived in [10]. Some general results on the functionals J for $\alpha_1 = 1$ in (2) can be found in [1] in a continuous setting.

For φ we can also use the *scaled Huber function*

$$\varphi(t) := \begin{cases} \frac{t^2}{2\alpha_2} & \text{if } |t| \leq \alpha_2, \\ |t| - \frac{\alpha_2}{2} & \text{if } |t| > \alpha_2 \end{cases} \quad \text{with} \quad \varphi'(t) = \begin{cases} \frac{t}{\alpha_2} & \text{if } |t| \leq \alpha_2, \\ \text{sign}(t) & \text{if } |t| > \alpha_2. \end{cases} \quad (3)$$

Note that the functions ψ and φ in Table 1 and (3) are nearly affine beyond a small neighborhood of the origin.

In this paper, we focus on the neighborhoods $\mathcal{N}4$ and $\mathcal{N}8$ depicted in Fig. 3 top. When taking the gradient of the functional in (1) we have to take into account that the pixel combination $u[i] - u[j]$ appears for $j \in \mathcal{N}_i^2$, where \mathcal{N}_i^2 denotes the “double” neighborhood associated with \mathcal{N}_i in Fig. 3 bottom. The usual choices are (see e. g. [8])

$$\begin{aligned} \gamma_{i,j} &:= 1 && \text{for vertical and horizontal neighbors,} \\ \gamma_{i,j} &:= \frac{1}{\sqrt{2}} && \text{for diagonal neighbors.} \end{aligned} \quad (4)$$

In all cases we have $\gamma_{i,j} = \gamma_{j,i}$.

Functionals of the form (1) with functions $\psi, \varphi \in \mathcal{C}^s$, $s \geq 2$ having alike properties (e.g. all functions in Table 1) were successfully used in [11] to process digital images f so that the obtained minimizer \hat{u} is quite close to the input digital image but its pixels can be ordered in a strict way. An analysis of the minimizers \hat{u} of these functionals has shown that with a probability close to one, \hat{u} has pixel values that are different from each other and different from the input pixels.

3 Bounds for the ℓ_∞ -Error

In this section, we give upper and lower estimates for the ℓ_∞ -error between the input image f and the image \hat{u} obtained by minimizing the functional $J(\cdot, f)$.

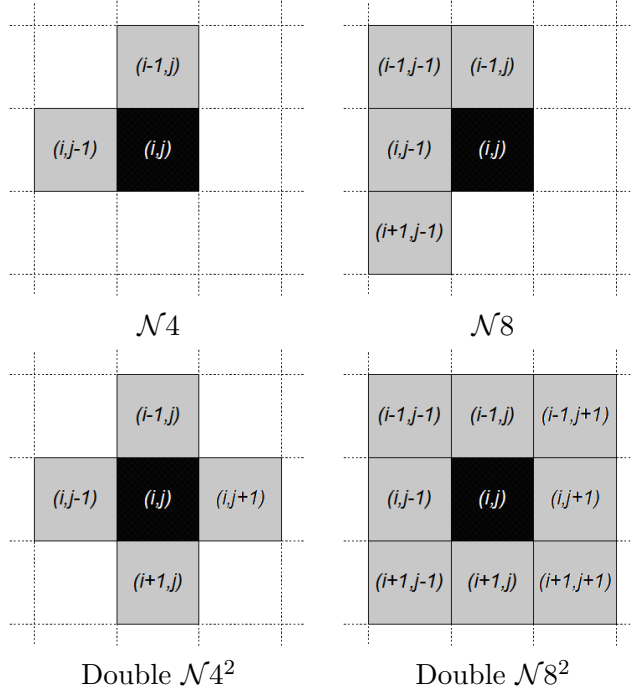


Figure 3: Neighborhoods $\mathcal{N}4$ (left) and $\mathcal{N}8$ (right) of a pixel (i, j) are used to formulate $\Phi(u)$. The double neighborhoods $\mathcal{N}4^2$ and $\mathcal{N}8^2$ appear in the gradient of $\Phi(u)$, see (7).

If \hat{u} is a minimizer of $u \mapsto J(u, f)$ we denote by $h \in \mathbb{R}^n$ the vector with components

$$h[i] := \sum_{j \in \mathcal{N}_i^2} \gamma_{i,j} \varphi'(\gamma_{i,j}(\hat{u}[i] - \hat{u}[j])), \quad i \in \mathbb{I}_n. \quad (5)$$

First we provide a lemma which gives a useful expression for $\|\hat{u} - f\|_\infty$.

Lemma 1 *Let H0, H1 $^\psi$ and H1 $^\varphi$ be satisfied. Let \hat{u} be the minimizer of $u \mapsto J(u, f)$ and h be given by (5). Then*

$$\|\hat{u} - f\|_\infty = (\psi')^{-1}(\beta \|h\|_\infty, \alpha_1). \quad (6)$$

Proof. In this proof we can omit the parameter α_1 . Using the definition of J and taking into account that φ' is odd, we have

$$\frac{\partial \Psi}{\partial u[i]} = \psi'(u[i] - f[i]) \quad \text{and} \quad \frac{\partial \Phi}{\partial u[i]} = \sum_{j \in \mathcal{N}_i^2} \gamma_{i,j} \varphi'(\gamma_{i,j}(u[i] - u[j])). \quad (7)$$

The minimizer \hat{u} of $J(\cdot, f)$ has to satisfy $\nabla_u J(\hat{u}, f) = 0$ which can be rewritten as $\nabla_u \Psi(\hat{u}, f) = -\beta \nabla \Phi(\hat{u})$ or as

$$\psi'(\hat{u}[i] - f[i]) = -\beta \sum_{j \in \mathcal{N}_i^2} \gamma_{i,j} \varphi'(\gamma_{i,j}(\hat{u}[i] - \hat{u}[j])), \quad i \in \mathbb{I}_n.$$

Using (5), the latter is equivalent to

$$\psi'(\hat{u}[i] - f[i]) = -\beta h[i], \quad i \in \mathbb{I}_n.$$

Since ψ' is by H0 and H1 $^\psi$ odd and strictly increasing,

$$\psi'(|\hat{u}[i] - f[i]|) = |\psi'(\hat{u}[i] - f[i])| = \beta |h[i]|. \quad (8)$$

Using Remark 1ii), we see that (8) is equivalent to

$$|\hat{u}[i] - f[i]| = (\psi')^{-1}(\beta |h[i]|) \quad (9)$$

where $(\psi')^{-1}$ is strictly increasing, hence

$$\|\hat{u} - f\|_\infty = \max_{i \in \mathbb{I}_n} (\psi')^{-1}(\beta |h[i]|) = (\psi')^{-1}(\beta \|h\|_\infty) .$$

□

For inner points $i \in \mathbb{I}_n^{\text{int}}$ we define

$$\eta := \sum_{j \in \mathcal{N}_i^2} \gamma_{i,j} . \quad (10)$$

Of course η does not depend on i but just on the choice of the neighborhood. If the weights are defined as in (4), we have

$$\begin{aligned} \eta &= 4 && \text{for } \mathcal{N}4 , \\ \eta &= 4 + \frac{4}{\sqrt{2}} = 6.8284 && \text{for } \mathcal{N}8 . \end{aligned}$$

For $i \in \mathbb{I}_n \setminus \mathbb{I}_n^{\text{int}}$ we have $\sum_{j \in \mathcal{N}_i^2} \gamma_{i,j} \leq \eta$ whose value depends on the boundary conditions.

In order to extend the obtained result, we shall use a property of $(\psi')^{-1}$ which is stated below.

Lemma 2 *Let ψ satisfy H0 , H1 $^\psi$ and H2 $^\psi$. Set*

$$\tilde{Y} := \min\{Y, \psi'(T)\} ,$$

where $\psi'(T) := \lim_{t \rightarrow +\infty} \psi'(t)$ if $T = +\infty$. Then for any $y \in (0, \tilde{Y})$, the function $\alpha_1 \mapsto (\psi')^{-1}(y, \alpha_1)$ is strictly increasing on $(0, +\infty)$.

Proof. Let $0 < a_1 < a_2$ and $y \in (0, \tilde{Y})$ be arbitrarily fixed. Since $t \mapsto \psi'(t, \alpha_1)$ is one-to-one and odd, there exist $t_1, t_2 \in (0, T)$ such that

$$\psi'(t_1, a_1) = y = \psi'(t_2, a_2) . \quad (11)$$

Thus we have $(\psi')^{-1}(y, a_1) = t_1$ and $(\psi')^{-1}(y, a_2) = t_2$. From H1 $^\psi$, $t \mapsto \psi'(t, \alpha_1)$ is strictly increasing for any fixed $\alpha_1 > 0$ and from H2 $^\psi$, $\alpha_1 \mapsto \psi'(t, \alpha_1)$ is strictly decreasing for any fixed $t \in (0, T)$. Therefore

$$t_2 \leq t_1 \quad \Rightarrow \quad y = \psi'(t_1, a_1) > \psi'(t_1, a_2) \geq \psi'(t_2, a_2) .$$

This contradicts (11). Consequently, $t_1 < t_2$ which implies the assertion. □

For all functions in Table 1 and for ψ in (2) we have $\tilde{Y} = 1$.

The following theorem provides an upper bound for $\|\hat{u} - f\|_\infty$ which is independent of f as well as of the particular shape of $\varphi(t, \alpha_2)$ provided that the latter meets the relevant assumptions.

Theorem 1 *Assume that H0 , H1 $^\psi$ and H1 $^\varphi$ are satisfied. Let $\beta \eta < Y$, where η is given in (10). Then the minimizer \hat{u} of $u \mapsto J(u, f)$ satisfies*

$$\|\hat{u} - f\|_\infty \leq (\psi')^{-1}(\beta \eta, \alpha_1) =: b(\beta, \alpha_1) . \quad (12)$$

If, in addition, ψ fulfills H2 $^\psi$ and $\beta \eta < \tilde{Y}$, where $\tilde{Y} = \min\{Y, \psi'(T)\}$, then $\alpha_1 \mapsto b(\beta, \alpha_1)$ is strictly increasing on $(0, +\infty)$.

Proof. From $H1^\varphi$, φ' is increasing with $|\varphi'(t)| \leq 1$ for any $t \in \mathbb{R}$. Inserting this into the definition of h in (5) yields

$$\|h\|_\infty \leq \eta. \quad (13)$$

Since $(\psi')^{-1}$ is by Remark 1ii) strictly increasing on $(0, Y)$, we deduce from (6) and (13) for $\beta\eta < Y$ that

$$\|\hat{u} - f\|_\infty = (\psi')^{-1}(\beta \|h\|_\infty, \alpha_1) \leq (\psi')^{-1}(\beta\eta, \alpha_1).$$

If ψ meets $H2^\psi$ and $\beta\eta < \tilde{Y}$ we obtain by Lemma 2 that the function $\alpha_1 \mapsto (\psi')^{-1}(\beta\eta, \alpha_1)$ is strictly increasing on $(0, +\infty)$. \square

We clarify the statement of Theorem 1 below.

- By Remark 1, the function $\beta \mapsto b(\beta, \alpha_1)$ is strictly increasing since η is a fixed number.
- The equality in (12) can only be met if φ' attains the limit in $H1^\psi$, i.e., if $\varphi'(t) = 1$ for some $t \in \mathbb{R}$. This is for example the case for the scaled Huber function in (3).
- The bound in (12) depends only on $\psi(\cdot, \alpha_1)$ and on β but it is independent of the selection of φ provided that $H1^\varphi$ holds.
- For all functions ψ listed in Table 1 we have $Y = 1$ which limits the action of β to less than $1/\eta$. So $H2^\psi$ furnishes a flexible tool to control the upper bound $b(\beta, \alpha_1)$ by using α_1 under the condition that $\beta\eta < \tilde{Y}$, where we remind that $\tilde{Y} = 1$ for all ψ in Table 1 and in (2).

The lower bound on $\|\hat{u} - f\|_\infty$ exhibited in the next Theorem 2 depends on $\varphi(t, \alpha_2)$ and on the input image f as well. In our formula, the reliance on f is expressed via the magnitude ν_f defined below:

$$\begin{aligned} \mathcal{I} &:= \{i \in \mathbb{I}_n^{\text{int}} \mid \text{sign}(f[i] - f[j]) = \sigma, \forall j \in \mathcal{N}_i \text{ where } \sigma \in \{-1, +1\}\}, \\ \nu_f &:= \max_{i \in \mathcal{I}} \min_{j \in \mathcal{N}_i} (\gamma_{i,j} |f[i] - f[j]|), \end{aligned} \quad (14)$$

where we set $\nu_f := 0$ if $\mathcal{I} = \emptyset$. The values of ν_f for some real-world images can be seen in Fig. 7.

Theorem 2 *Let $H0$, $H1^\psi$, $H2^\psi$ and $H1^\varphi$, $H2^\varphi$ be verified. Let $\beta\eta < Y$, where η is given in (10). Assume that $\nu_f > 2b(\beta, \alpha_1)$. Then the minimizer \hat{u} of $u \mapsto J(u, f)$ fulfills*

$$\|\hat{u} - f\|_\infty \geq (\psi')^{-1}(c\beta\eta, \alpha_1) =: \ell(\beta, \alpha_1, \alpha_2, \nu_f), \quad (15)$$

where

$$c = c(\beta, \alpha_1, \alpha_2, \nu_f) := \varphi'(\nu_f - 2b(\beta, \alpha_1), \alpha_2) \leq 1.$$

The function $\alpha_2 \mapsto \ell(\beta, \alpha_1, \alpha_2, \nu_f)$ is decreasing on $(0, +\infty)$ and

$$\ell(\beta, \alpha_1, \alpha_2, \nu_f) \nearrow b(\beta, \alpha_1) \text{ as } \alpha_2 \searrow 0. \quad (16)$$

Moreover, for $\varepsilon > 0$ arbitrarily close to zero, α_2 can be set so that

$$\|\hat{u} - f\|_\infty \geq (\psi')^{-1}((1 - \varepsilon)\beta\eta, \alpha_1). \quad (17)$$

Proof. From the definition on ν_f , there exists $i \in \mathbb{I}_n^{\text{int}}$ such that

$$\gamma_{i,j} |f[i] - f[j]| \geq \nu_f, \quad \forall j \in \mathcal{N}_i.$$

We consider the case

$$\gamma_{i,j}(f[i] - f[j]) \geq \nu_f > 2b(\beta, \alpha_1), \quad \forall j \in \mathcal{N}_i. \quad (18)$$

The opposite case, namely $\gamma_{i,j}(f[j] - f[i]) \geq \nu_f > 2b(\beta, \alpha_1), \forall j \in \mathcal{N}_i$ can be handled in the same way. By Theorem 1, the minimizer \hat{u} of $J(\cdot, f)$ meets

$$\begin{aligned} -b(\beta, \alpha_1) &\leq \hat{u}[i] - f[i], \\ -b(\beta, \alpha_1) &\leq f[j] - \hat{u}[j], \quad \forall j \in \mathcal{N}_i. \end{aligned}$$

Thus

$$\begin{aligned} -2b(\beta, \alpha_1) &\leq \hat{u}[i] - \hat{u}[j] - (f[i] - f[j]), \quad \forall j \in \mathcal{N}_i, \\ -2b(\beta, \alpha_1) + (f[i] - f[j]) &\leq \hat{u}[i] - \hat{u}[j], \quad \forall j \in \mathcal{N}_i. \end{aligned} \quad (19)$$

Combining (18) and (19) along with the fact that $\gamma_{i,j} \leq 1$ yields

$$0 < -2b(\beta, \alpha_1) + \nu_f \leq -2b(\beta, \alpha_1) + \gamma_{i,j}(f[i] - f[j]) \leq \gamma_{i,j}(\hat{u}[i] - \hat{u}[j]) \quad \forall j \in \mathcal{N}_i.$$

Since $t \mapsto \varphi'(t, \alpha_2)$ is increasing by H1 $^\varphi$, the value $h[i]$ in (5) satisfies

$$h[i] \geq \sum_{j \in \mathcal{N}_i^2} \gamma_{i,j} \varphi'(\nu_f - 2b(\beta, \alpha_1), \alpha_2) = \eta c(\beta, \alpha_1, \alpha_2, \nu_f).$$

Using yet again that $y \mapsto (\psi')^{-1}(y, \alpha_1)$ is strictly increasing (Remark 1ii)) we obtain by (9) that

$$|\hat{u}[i] - f[i]| \geq (\psi')^{-1}(c\beta\eta, \alpha_1) = \ell(\beta, \alpha_1, \alpha_2, \nu_f).$$

Since $\|\hat{u} - f\|_\infty \geq |\hat{u}[i] - f[i]|$, it follows that

$$\|\hat{u} - f\|_\infty \geq (\psi')^{-1}(c\beta\eta, \alpha_1).$$

Using H2 $^\varphi$, the function $\alpha_2 \mapsto c(\beta, \alpha_1, \alpha_2, \nu_f)$ is continuous and decreasing on $(0, +\infty)$ and $\lim_{\alpha_2 \searrow 0} c(\beta, \alpha_1, \alpha_2, \nu_f) = 1$. Combining the latter with Remark 1ii) entails that $\alpha_2 \mapsto \ell(\beta, \alpha_1, \alpha_2, \nu_f)$ is decreasing on $(0, +\infty)$. Then the definition of $b(\beta, \alpha_1)$ in (12) leads to (16).

Finally, H2 $^\varphi$ shows that for ε arbitrarily close to zero there is $\alpha_2 > 0$ such that $c(\beta, \alpha_1, \alpha_2, \nu_f) = (1 - \varepsilon)$ and consequently $\|\hat{u} - f\|_\infty \geq (\psi')^{-1}((1 - \varepsilon)\beta\eta)$. \square

Some comments on Theorem 2 may be useful.

- The expression in (17) tells us that by decreasing α_2 , the lower bound $\ell(\cdot)$ can be adjusted arbitrarily close to the upper bound $b(\cdot)$. The amount of decrease of α_2 needed to reach $(1 - \varepsilon)$ depends on the input image f and can be calculated.
- If $t \mapsto \varphi'(t, \alpha_2)$ is *nonstrictly* increasing on $[0, +\infty)$, as the Huber function in (3), it is easy to see that there is α_2 such that $c(\beta, \alpha_1, \alpha_2, \nu_f) = 1$ and hence $\ell(\beta, \alpha_1, \alpha_2, \nu_f) = b(\beta, \alpha_1)$.

4 Explicit Parameter Estimates

In this section we want to use the error bounds from the previous section to give explicit parameter estimates of β , α_1 and α_2 for the functions ψ , φ mentioned in Section 2. More precisely, for a given β satisfying a constraint and for δ fixed, we exhibit the value $\alpha_1 = \hat{\alpha}_1$ ensuring that $b(\beta, \hat{\alpha}_1) = \delta$ and then calculate $\ell(\beta, \hat{\alpha}_1, \alpha_2, \nu_f)$.

For the functions ψ in Table 1 and in (2) we have $\tilde{Y} = 1$. When the weights $\gamma_{i,j}$ are chosen as in (4) and $H2^\psi$ holds, the assumption $\beta\eta < \tilde{Y} = 1$ in Theorem 1 reads

$$\begin{aligned} \beta < \frac{1}{4} = 0.25 & \quad \text{for } \mathcal{N}4, \\ \beta < \frac{1}{6.8284} = 0.1464 & \quad \text{for } \mathcal{N}8. \end{aligned} \tag{20}$$

In the following we choose $\beta > 0$ such that $\beta < \frac{1}{\eta}$. For $\delta > 0$ fixed, let $\hat{\alpha}_1$ solve the equation

$$b(\beta, \alpha_1) = (\psi')^{-1}(\beta\eta, \alpha_1) = \delta. \tag{21}$$

Then we have by Theorem 1 that $\|\hat{u} - f\|_\infty \leq \delta$ for all $\alpha_1 \in (0, \hat{\alpha}_1]$ and there does not exist $\alpha_1 > \hat{\alpha}_1$ such that $\|\hat{u} - f\|_\infty \leq \delta$ holds true. In this sense we call $\hat{\alpha}_1$ *optimal for δ* . This claim is ensured thanks to $H2^\psi$ which guarantees that $\alpha_1 \mapsto b(\beta, \alpha_1)$ is strictly increasing (see Lemma 2). The value c in Theorem 2 depends on φ and on f via ν_f . Given the input image f the constant ν_f is easy to compute. When

$$z := \nu_f - 2b(\beta, \alpha_1) > 0,$$

Theorem 2 indicates that the constant c reads

$$c = \varphi'(z, \alpha_2). \tag{22}$$

In our experiments on real-world digital images, we always had $z \gg 0$ for $\delta = 0.5$. By Theorem 2 a sharper lower bound requires a smaller value for α_2 . According to Theorem 1 and Theorem 2, the upper and lower bounds for $\|f - \hat{u}\|_\infty$ and the optimal value for α_1 as defined in (21) for the functions ψ in Table 1 and in (2) are given in Table 2.

$\psi(t)$	$b(\beta, \alpha_1)$	$\ell(\beta, \alpha_1, \alpha_2, \nu_f)$	$\hat{\alpha}_1$
$\sqrt{t^2 + \alpha_1}$	$\sqrt{\frac{\alpha_1(\beta\eta)^2}{1 - (\beta\eta)^2}}$	$\sqrt{\frac{\alpha_1(c\beta\eta)^2}{1 - (c\beta\eta)^2}}$	$\delta^2 \left(\frac{1}{\beta^2\eta^2} - 1 \right)$
$ t - \alpha_1 \log \left(1 + \frac{ t }{\alpha_1} \right)$	$\frac{\alpha_1 \beta\eta}{1 - \beta\eta}$	$\frac{\alpha_1 c\beta\eta}{1 - c\beta\eta}$	$\delta \left(\frac{1}{\beta\eta} - 1 \right)$
$\alpha_1 \log \left(\cosh \left(\frac{t}{\alpha_1} \right) \right)$	$\alpha_1 \operatorname{atanh}(\beta\eta)$	$\alpha_1 \operatorname{atanh}(c\beta\eta)$	$\frac{\delta}{\operatorname{atanh}(\beta\eta)}$
$\frac{1}{\alpha_1 + 1} t ^{\alpha_1 + 1}$	$(\beta\eta)^{\frac{1}{\alpha_1}}$	$(c\beta\eta)^{\frac{1}{\alpha_1}}$	$\frac{\ln(\beta\eta)}{\ln \delta}$

Table 2: Bounds and parameter $\hat{\alpha}_1$ for various functions ψ in Table 1 and in (2). The parameter c depends on φ' by (22). The allowed values for β by Theorem 1 are given in (20).

If $\delta = 0.5$ then \hat{u} has the important property that it preserves the order of the pixel values in a digital image $f \in \{0, \dots, L-1\}^n$. The corresponding values $\hat{\alpha}_1$ and β are presented in Table 3.

Remark 2 Equation (21) offers several other exploits than only fixing the optimal $\hat{\alpha}_1$. For any $\beta < \frac{Y}{\eta}$ one can also

$\psi(t)$	$\sqrt{t^2 + \alpha_1}$		$ t - \alpha_1 \log \left(1 + \frac{ t }{\alpha_1} \right)$	
neighborhood	β	$\hat{\alpha}_1$	β	$\hat{\alpha}_1$
\mathcal{N}_4	0.2	0.1406	0.2	0.1250
\mathcal{N}_4	0.1	1.3125	0.1	0.7500
\mathcal{N}_8	0.1	0.2862	0.1	0.2322
\mathcal{N}_8	0.05	1.8947	0.05	0.9645

Table 3: Allowed values $\beta < 1/\eta$ and the optimal $\hat{\alpha}_1$ for $\delta = b(\beta, \hat{\alpha}_1) = 0.5$.

- calculate δ when α_1 and β are given—this can be useful e.g. when ℓ_1 -TV or ℓ_2 -TV are approximated by a fully smooth functional;
- determine the optimal β for fixed α_1 and δ —we remind that from Remark 1, $\beta \mapsto b(\beta, \alpha_1)$ is strictly increasing, hence this value of β is unique.

5 Probability Estimates for Pixel Neighborhoods

Consider that the assumptions H_0 , H_1^ψ , H_1^φ and H_2^φ are met and that the parameters $\beta < Y/\eta$, α_1 and α_2 are fixed. From Theorem 2 we know that the upper bound $b(\beta, \alpha_1)$ in Theorem 1 provides a nearly perfect approximation of the true error $\|\hat{u} - f\|_\infty$ when $c = \varphi'(\nu_f - 2b, \alpha_2)$ is close to one, which by H_1^φ means that ν_f is large enough. In order to get an intuition—even though very rough—on the behaviour of ν_f , we assume in this section that the values of f are realizations of a discrete random variable X taking values in $\{0, \dots, L-1\}$ whose probability density function (pdf) p_X is specialized to real-world digital images. Fig. 4 shows an image together with its histogram which furnishes an empirical estimate of the corresponding pdf.

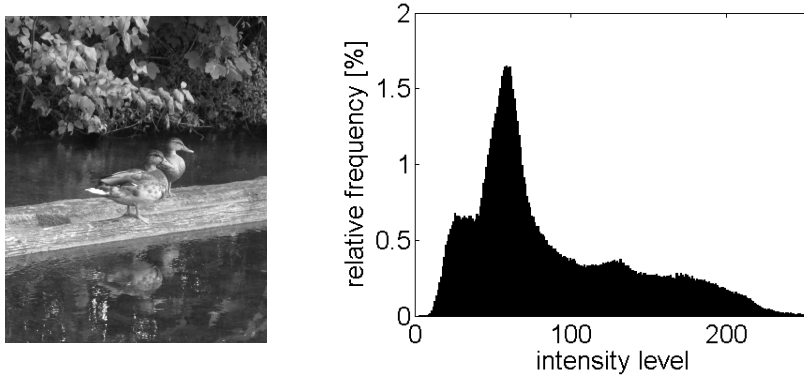


Figure 4: Left: Duck image. Right: Histogram of “duck image” furnishing an empirical estimate of the corresponding pdf.

First, we ask for the probability that an inner image pixel $i \in \mathbb{I}_n^{\text{int}}$ fulfills

$$|f[i] - f[j]| \geq a \text{ and } \text{sign}(f[i] - f[j]) = \sigma, \quad \forall j \in \mathcal{N}_i \quad (23)$$

where $\sigma \in \{-1, +1\}$ and $a > 0$ is fixed.

Lemma 3 *Let $X, X_i, i = 1, \dots, k$ be independent and identically distributed (iid) discrete random variables taking values in $\{0, \dots, L-1\}$. Then it holds for $a > 0$ that*

$$q(X, k, a) := P(X - X_1 \geq a, \dots, X - X_k \geq a) = \sum_{i=0}^{L-1} (P(X \leq i - a))^k P(X = i). \quad (24)$$

Proof. Since the random variables are iid we obtain

$$\begin{aligned} P(X - X_1 \geq a, \dots, X - X_k \geq a) &= \sum_{i=0}^{L-1} (P(i - X_1 \geq a, \dots, i - X_k \geq a, X = i)) \\ &= \sum_{i=0}^{L-1} (P(X \leq i - a))^k P(X = i). \quad \square \end{aligned}$$

A case relevant to our context is when X is a given inner pixel and X_i for $i \in \{1 \dots, k\}$ are the pixels in the “double” neighborhood of X , see Fig. 3. Then the setting of Lemma 3 considers neighborhoods where the central pixel X is bigger than all its neighbors by at least the amount of a . It is clear that the opposite case (when $X - X_i \leq -a$ for all $i \in 1 \dots, k$) is of the same interest and appears with the same probability $P(X - X_1 \leq -a, \dots, X - X_k \leq -a) = q(X, k, a)$. Of course the “iid” assumption is not realistic for natural images.

For $k = 1$, the probabilities $P(X - X_1 \geq a)$ and $P(X - X_1 \leq -a)$ can be easily exemplified. Let X and X_1 follow independently the same pdf p_X . In order to obtain the joint pdf of X and X_1 , one has to compute $P(X = i_1)P(X = i_2)$ for all gray levels i_1, i_2 obeying $|i_1 - i_2| \geq a$ and then take their sum. Fig. 5 (left) shows for example the joint pdf of X and X_1 when X and X_1 are iid random variables following the pdf p_X of the “ducks image” in Fig. 4 left. At position $(i_1, i_2) \in \{0, \dots, 255\}^2$ the probability $P(X = i_1)P(X_1 = i_2)$ is visualized as a gray value where lighter areas correspond to higher probability.

In Fig. 5 (right) the shaded areas show the points where the pixel difference $|i_1 - i_2|$ is larger or equal to a . The sum of the probabilities corresponding to these areas is $2q(X, 1, a)$.

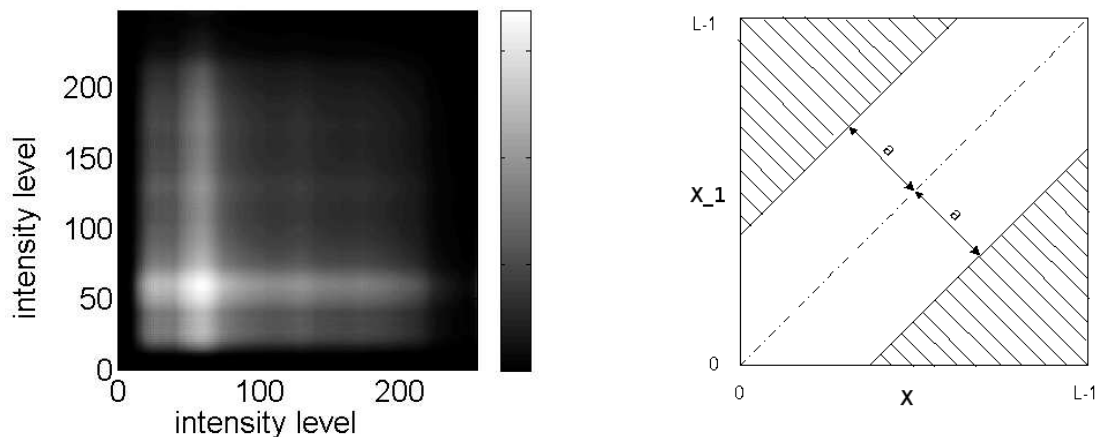


Figure 5: Left: Joint pdf of two iid random variables X, X_1 where X and X_1 follow the pdf of the “ducks image” in Fig. 4 right. Here light areas correspond to high probability. Right: Areas where $|i_1 - i_2| \geq a$, $i_1, i_2 \in \{0, \dots, L - 1\}$. The value $2q(X, 1, a)$ is the sum of the probabilities in the shaded areas.

Theorem 3 Assume that the $M \times N$ image f is the realization of a discrete iid random vector $(X_i)_{i=1}^n$ with iid components X_i as X , where $n = MN$. Let ν_f be defined as in (14) with respect to $\mathcal{N}4$. Then the probability that $\nu_f \geq a > 0$ is not smaller than

$$1 - (1 - 2q(X, 4, a))^m, \quad (25)$$

where q is defined in (24) and $m = \lfloor M/3 \rfloor \times \lfloor N/3 \rfloor$.

For $\mathcal{N}8$ we have to replace q by $\tilde{q}(X, 4, a) := \sum_{i=0}^{L-1} (P(X \leq i - a))^4 (P(X \leq i - \sqrt{2}a))^4 P(X = i)$.

Proof. We consider only inner pixels i with non-overlapping neighborhoods as depicted in Fig. 6. Then, by Lemma 3, the probability that one of these pixels does not verify (23) is given by $1 - 2q(X, 4, a)$. Hence the probability that all these inner pixels do not fulfill (23) is $(1 - 2q(X, 4, a))^m$ and the probability that at least one of these pixel satisfies (23) is $1 - (1 - 2q(X, 4, a))^m$. \square

Note that for $q(X, 4, a) > 0$ the probability in (25) is indeed very close to 1 even for moderate sizes of m . For instance, if the random variables are *uniformly* iid, we have

$$q(X, 4, a) = \frac{1}{L} \sum_{i=a}^{L-1} \left(\frac{i-a+1}{L} \right)^4 = \frac{(L-a)(L-a+1)(2(L-a)+1)(3(L-a)^2+3(L-a)-1)}{30L^5}.$$

For $a = 137$ and $L = 256$ this formula gives $q(X, 4, a) \approx 0.0044$ and for $M = N = 128$ further $1 - (1 - q(X, 4, a))^m \approx 1 - 10^{-7}$.

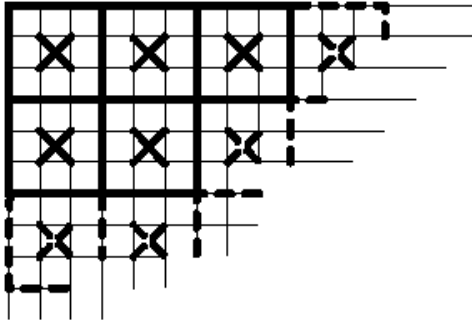


Figure 6: Disjoint 3×3 -adjacencies with center pixels “x”.

6 Numerical Tests

The bounds on $\|\hat{u} - f\|_\infty$ with respect to the model parameters were tested on a wide amount of images. Here we present the results on 15 digital images of different sizes, with gray values in $\{0, \dots, 255\}$, available at <http://sipi.usc.edu/database/>. In our selection the images have various quality and content (presence or quasi-absence of edges, textures, nearly flat regions). They are displayed in Fig. 7. The values of ν_f for $\mathcal{N}8$ under each image shows that the assumption $\nu_f - 2b(\beta, \alpha_1) > 0$ in Theorem 2 is generously satisfied in all these cases as far as we are interested to fix $b(\beta, \alpha_1) \leq 0.5$. We also performed tests with 10^4 random 256×256 images with pixel values uniformly distributed in $\{0, \dots, 255\}$. For $\mathcal{N}4$ we obtained $\text{mean}(\nu_f) = 224.2267$ and for $\mathcal{N}8$, $\text{mean}(\nu_f) = 137.7871$.

We tested two functionals $J(\cdot, f)$ as described in Section 2: the first corresponds to $\psi = \Theta 1$ and $\varphi = \Theta 1$ and the second to $\psi = \Theta 2$ and $\varphi = \Theta 1$ as given in Table 1. In all tests, $\mathcal{N}8$ was adopted with the weights $\gamma_{i,j}$ given in (4). Two choices for β satisfying (20) were considered along with different values for α_1 and α_2 . The minimizers \hat{u} were computed using Polak-Ribière conjugated gradients [3] with high numerical precision. For each restored image we computed $\|\hat{u} - f\|_\infty$ and present the distance between the theoretical upper bound $b(\beta, \alpha_1)$ and the obtained $\|\hat{u} - f\|_\infty$:

$$b(\beta, \alpha_1) - \|\hat{u} - f\|_\infty.$$

The tables show also the difference between the upper and the lower theoretical bounds on $\|\hat{u} - f\|_\infty$:

$$b - \ell := b(\beta, \alpha_1) - \ell(\beta, \alpha_1, \alpha_2, \nu_f),$$

computed using the explicit formulae given in Section 4. Furthermore, we evaluate the amount of pixels that closely approach the ℓ_∞ norm:

$$q = \# \{i \in \mathbb{I}_n \mid \|\hat{u} - f\|_\infty - |\hat{u}[i] - f[i]| < \varepsilon\} \quad \text{and} \quad Q\% = 100 \frac{q}{n},$$

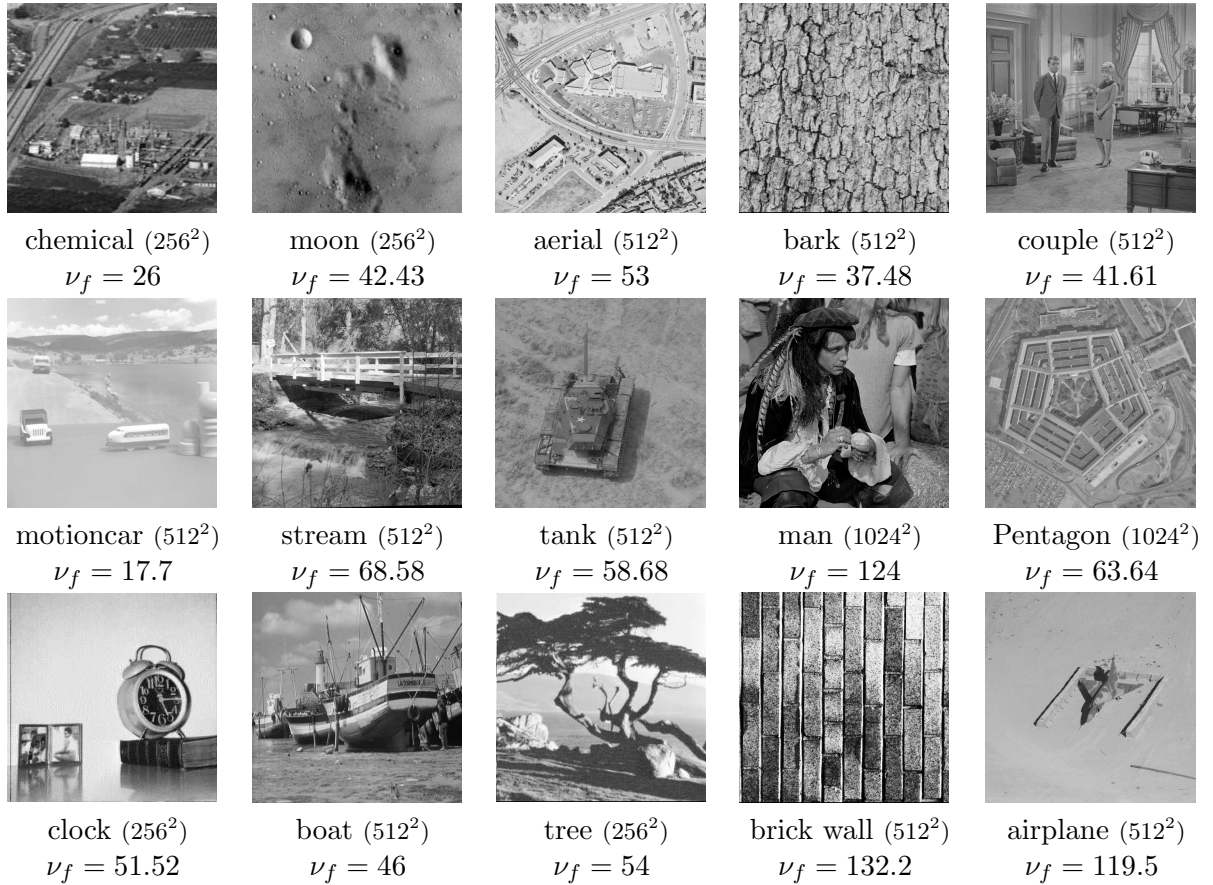


Figure 7: The set of images used in the tests provided in this section. The values of ν_f are computed according to (14) in the case $\mathcal{N}8$ for the weights in (4).

$\mathcal{N}8$, $\psi(t) = \sqrt{t^2 + \alpha_1}$ for $\alpha_1 = 0.2862$, $\beta = 0.1$ hence $b = 0.5$, $\varphi(t) = \sqrt{t^2 + \alpha_2}$

image	$\alpha_2 = 0.02$			$\alpha_2 = 100$		
	$b - \ \hat{u} - f\ _\infty \times 10^{-6}$	$b - \ell \times 10^{-6}$	Q %	$b - \ \hat{u} - f\ _\infty \times 10^{-3}$	$b - \ell \times 10^{-2}$	q
chemical	4.764	14.90	4.04	22.85	6.143	2
moon	2.438	5.459	9.27	12.49	2.525	1
aerial	2.066	3.465	3.46	6.949	1.647	1
bark	2.977	7.041	6.57	13.44	3.188	1
couple	2.485	2.568	3.25	12.77	2.619	4
motioncar	19.98	33.68	0.18	77.56	11.35	1
stream	0.918	2.051	7.14	5.412	0.995	2
tank	1.960	2.815	6.95	9.297	1.351	1
man	0.025	0.619	4.94	1.581	0.307	8
Pentagon	1.181	2.388	9.12	6.368	1.153	1
clock	2.079	3.671	2.88	6.884	1.740	1
boat	1.707	4.626	6.04	8.425	2.164	2
tree	1.202	3.325	5.27	8.026	1.584	1
brick wall	0.334	0.544	11.8	1.842	0.270	43
airplane	0.412	0.667	1.73	2.089	0.330	1

Table 4: Results for $\psi = \Theta 1$, $\varphi = \Theta 1$, $\beta = 0.1$ and a small and large value of α_2 , respectively. Over the whole set of these images, for $\alpha_2 = 0.02$ we have $\text{mean}(0.5 - \|\hat{u} - f\|_\infty) = 2.968 \times 10^{-6}$ and $\text{mean}(0.5 - \ell(\beta, \alpha_1, \alpha_2, \nu_f)) = 6.0678 \times 10^{-6}$. For $\alpha_2 = 100$ these values read $\text{mean}(0.5 - \|\hat{u} - f\|_\infty) = 1.307 \times 10^{-2}$ and $\text{mean}(0.5 - \ell(\beta, \alpha_1, \alpha_2, \nu_f)) = 2.491 \times 10^{-2}$.

where $\#$ stands for cardinality and $\varepsilon \gtrsim 0$ in order to account for numerical errors. In the experiments, we set $\varepsilon := 10^{-3}$.

In all tests, given $0 < \beta < 1/\eta$, we fixed $\alpha_1 = \hat{\alpha}_1$ so that

$$b(\beta, \hat{\alpha}_1) = \delta \quad \text{for} \quad \delta = \frac{1}{2}.$$

The numerical outcomes confirm the theoretical results on $\|\hat{u} - f\|_\infty$ established in Sections 3 and 4. From Tables 4, 5 and 6 the following observations can be drawn:

- Decreasing $\alpha_2 > 0$ towards 0 enables to make the difference between the upper and the lower bounds on $\|\hat{u} - f\|_\infty$ arbitrarily small which leads to $\|u - f\|_\infty \approx b(\beta, \alpha_1)$.

In this case a large percentage of the pixels i meet $|\hat{u}[i] - f[i]| \approx b(\beta, \alpha_1)$.

- An important increase of $\alpha_2 > 0$ entails a decrease of the lower bound $\ell(\beta, \alpha_1, \alpha_2, \nu_f)$. Moreover, the number of pixels i verifying $|\hat{u}[i] - f[i]| \approx b(\beta, \alpha_1)$ is reduced to a few ones.

Such a situation may be preferable when one wishes that there are not too many pixels close to the upper bound.

Tables 7 and 8 show yet again that the gap between the upper bound $b(\beta, \alpha_1)$ and the lower bound $\ell(\beta, \alpha_1, \alpha_2, \nu_f)$ vanishes when α_2 is close to zero and that it increases when α_2 increases. For α_2 fixed, we see that $b(\beta, \alpha_1) - \ell(\beta, \alpha_1, \alpha_2, \nu_f)$ tends to decrease along with β .

Fig. 8 shows the histograms of the differences $\{f[i] - \hat{u}[i], i \in \mathbb{I}_n\}$ relevant to “moon”, where the upper bound was set to $b(\beta, \alpha_1) = 0.5$, for an increasing set of values of α_2 . These histograms were plotted for 100 bins equally spaced in $[-0.5, +0.5]$. For very small values of α_2 , there are many pixels meeting $|f[i] - \hat{u}[i]| \approx \|f - \hat{u}\|_\infty$. When α_2 increases, such pixels become more and more rare and the differences $|f[i] - \hat{u}[i]|$ become centered near zero. However they never reach zero: see the value of μ defined in the caption of the figure. Here again, the numerical tests were done with a high precision.

$\mathcal{N}8$, $\psi(t) = \sqrt{t^2 + \alpha_1}$ for $\alpha_1 = 1.895$, $\beta = 0.05$ hence $b = 0.5$, $\varphi(t) = \sqrt{t^2 + \alpha_2}$

image	$\alpha_2 = 0.02$			$\alpha_2 = 100$		
	$b - \ \hat{u} - f\ _\infty \times 10^{-6}$	$b - \ell \times 10^{-6}$	$Q\%$	$b - \ \hat{u} - f\ _\infty \times 10^{-3}$	$b - \ell \times 10^{-2}$	q
chemical	2.561	9.055	4.54	14.17	3.993	2
moon	1.580	3.300	10.2	7.649	1.572	1
aerial	0.872	2.093	3.92	4.229	1.015	2
bark	1.673	4.254	6.82	8.239	2.000	1
couple	1.642	3.432	3.25	7.830	1.632	4
motioncar	12.39	20.35	0.28	51.43	7.847	1
stream	0.727	1.240	7.19	3.291	0.608	3
tank	1.020	1.701	8.31	5.678	0.829	1
man	0.162	0.374	6.00	0.968	0.186	11
Pentagon	0.871	1.442	10.2	3.877	0.706	1
clock	1.013	2.220	2.88	4.193	1.073	1
boat	0.799	2.795	7.14	5.136	1.342	2
tree	0.993	2.009	6.06	4.895	0.975	2
brick wall	0.125	0.329	11.9	1.115	0.164	99
airplane	0.228	0.403	3.48	1.274	0.200	1

Table 5: Results for $\psi = \Theta 1$, $\varphi = \Theta 1$, $\beta = 0.05$ and a small and large value of α_2 , respectively. For $\alpha_2 = 0.02$ we have $\text{mean}(0.5 - \|\hat{u} - f\|_\infty) = 1.777 \times 10^{-6}$ and $\text{mean}(0.5 - \ell(\beta, \alpha_1, \alpha_2, \nu_f)) = 3.666 \times 10^{-6}$. For $\alpha_2 = 100$, we find $\text{mean}(0.5 - \|\hat{u} - f\|_\infty) = 8.265 \times 10^{-3}$ and $\text{mean}(0.5 - \ell(\beta, \alpha_1, \alpha_2, \nu_f)) = 1.610 \times 10^{-2}$.

$\mathcal{N}8$, $\psi(t) = |t| - \alpha_1 \log\left(1 + \frac{|t|}{\alpha_1}\right)$ for $\alpha_1 = 0.9645$, $\beta = 0.05$, hence $b = 0.5$, $\varphi(t) = \sqrt{t^2 + \alpha_2}$

image	$\alpha_2 = 0.05$			$\alpha_2 = 100$		
	$b - \ \hat{u} - f\ _\infty \times 10^{-6}$	$b - \ell \times 10^{-6}$	$Q\%$	$b - \ \hat{u} - f\ _\infty \times 10^{-3}$	$b - \ell \times 10^{-2}$	q
chemical	0.101	0.304	2.79	18.81	5.236	2
moon	5.347	11.06	7.03	10.22	2.090	1
aerial	2.670	7.019	2.63	5.663	1.354	2
bark	5.843	14.26	5.55	11.01	2.653	1
couple	5.369	11.51	3.25	10.46	2.170	4
motioncar	41.36	68.23	0.09	66.99	0.101	1
stream	1.687	4.155	6.66	4.404	0.813	3
tank	3.869	5.703	4.45	7.592	1.107	1
man	0.673	1.255	3.14	1.298	0.249	10
Pentagon	2.723	4.837	6.55	5.188	0.943	1
clock	2.622	7.437	2.88	5.610	1.431	1
boat	3.879	9.373	3.97	6.874	1.786	2
tree	4.070	6.737	4.18	6.549	1.301	2
brick wall	0.721	1.102	11.3	1.710	0.219	61
airplane	0.682	1.352	0.74	4.983	0.268	1

Table 6: Results for $\psi = \Theta 2$, $\varphi = \Theta 1$, $\beta = 0.05$ and a small and large value of α_2 , respectively. For $\alpha_2 = 0.05$ we have $\text{mean}(0.5 - \|\hat{u} - f\|_\infty) = 5.441 \times 10^{-6}$ and $\text{mean}(0.5 - \ell(\beta, \alpha_1, \alpha_2, \nu_f)) = 10.29 \times 10^{-6}$. For $\alpha_2 = 100$, we find $\text{mean}(0.5 - \|\hat{u} - f\|_\infty) = 1.09 \times 10^{-2}$ and $\text{mean}(0.5 - \ell(\beta, \alpha_1, \alpha_2, \nu_f)) = 2.11 \times 10^{-2}$.

mean $(b(\beta, \alpha_1) - \ell(\beta, \alpha_1, \alpha_2, \nu_f))$, $b(\beta, \alpha_1) = 0.5$, $\mathcal{N}8$				
	$\alpha_2 = 0.01$		$\alpha_2 = 100$	
	$\beta = 0.1$	$\beta = 0.05$	$\beta = 0.1$	$\beta = 0.05$
$\psi = \Theta 1, \varphi = \Theta 1$	3.034×10^{-6}	1.833×10^{-6}	2.491×10^{-2}	1.610×10^{-2}
$\psi = \Theta 2, \varphi = \Theta 1$	5.106×10^{-6}	2.459×10^{-6}	3.985×10^{-2}	2.112×10^{-2}
$\psi(t) = \frac{1}{\alpha_1+1} t ^{\alpha_1+1}, \varphi = \Theta 1$	2.994×10^{-6}	1.045×10^{-6}	2.542×10^{-2}	0.941×10^{-2}

Table 7: The mean value of the difference $b(\beta, \alpha_1) - \ell(\beta, \alpha_1, \alpha_2, \nu_f)$ was computed over the selection of images shown in Fig. 7. Here we consider the $\mathcal{N}8$ neighborhood for the weights in (4).

mean $(b(\beta, \alpha_1) - \ell(\beta, \alpha_1, \alpha_2, \nu_f))$, $b(\beta, \alpha_1) = 0.5$, $\mathcal{N}4$				
	$\alpha_2 = 0.01$		$\alpha_2 = 100$	
	$\beta = 0.2$	$\beta = 0.1$	$\beta = 0.2$	$\beta = 0.1$
$\psi = \Theta 1, \varphi = \Theta 1$	2.980×10^{-6}	1.278×10^{-6}	2.253×10^{-2}	1.104×10^{-2}
$\psi = \Theta 2, \varphi = \Theta 1$	5.364×10^{-6}	1.788×10^{-6}	3.780×10^{-2}	1.504×10^{-2}
$\psi(t) = \frac{1}{\alpha_1+1} t ^{\alpha_1+1}, \varphi = \Theta 1$	3.333×10^{-6}	0.812×10^{-6}	2.718×10^{-2}	0.722×10^{-2}

Table 8: The neighborhood here is $\mathcal{N}4$ with the weights given in (4). The mean is calculated over the set of images in Fig.7.

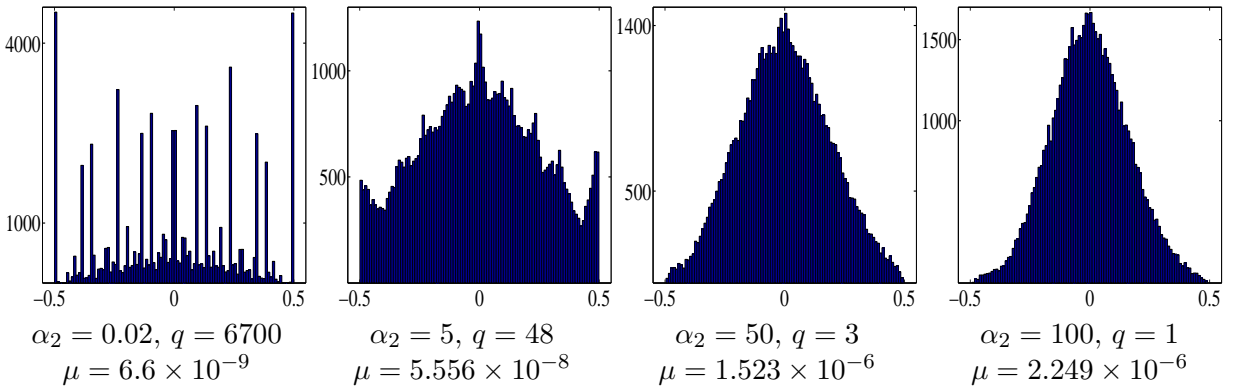


Figure 8: Histograms of $\{f[i] - \hat{u}[i], i \in \mathbb{I}_n\}$ for “moon” restored using $\psi = \Theta 1, \varphi = \Theta 1, \mathcal{N}8$, $\beta = 0.05$ and for different values of α_2 . The parameter $\alpha_1 = 1.8947$ was set so that $b(\beta, \alpha_1) = 0.5$. The image has $n = 65536$ pixels. The value μ is defined by $\mu := \min_{i \in \mathbb{I}_n} |f[i] - \hat{u}[i]|$.

7 Conclusions and Open Questions

ℓ_1 -TV and ℓ_2 -TV functionals have been often minimized using a smoothed version of the form we consider in this paper with ad hoc chosen smoothing parameters (“very small”). The results established in our work enable to clearly evaluate the resulting approximation.

The functions (ψ, φ) studied here have a lot of similarities. However, they produce different image restorations. The question of what couple of functions (ψ, φ) would give a better result in the framework of a given application, remains open.

Extension to the rotational-invariant (in a discrete sense) smoothed TV, i.e. $\Phi(u) = \sum_{i,j} \varphi(\|\nabla_{i,j}u\|)$, where $\nabla_{i,j}u \in \mathbb{R}^2$ stands for a discrete approximation of the gradient of u at pixel (i, j) , deserves attention.

Extensions to cases when f are the coefficients of the expansion of the input image using an orthogonal transform as the discrete cosine transform or a frame transform as the curvelet transform, see, e.g., [9] are of interest.

Applications to quantization noise reduction should be envisaged.

References

- [1] G. AUBERT AND P. KORNPORST, *Mathematical problems in image processing*, Springer-Verlag, Berlin, 2 ed., 2006.
- [2] A. BECK AND M. TEOULLE, *Smoothing and First Order Methods: A Unified Framework*, SIAM Journal on Optimization, 22(2) (2012), pp. 557–580.
- [3] J. F. BONNANS, J.-C. GILBERT, C. LEMARÉCHAL, AND C. A. SAGASTIZÁBAL, *Numerical Optimization (Theoretical and Practical Aspects)*, Springer, Berlin ; New York NY ; Hong Kong, 2003.
- [4] P. L. COMBETTES AND J.-C. PESQUET, *Proximal Splitting Methods in Signal Processing*, In “Fixed-Point Algorithms for Inverse Problems in Science and Engineering”, H. H. Bauschke, R. S. Burachik, P. L. Combettes, V. Elser, D. R. Luke and H. Wolkowicz (Eds.), Springer-Verlag, 2011, pp. 185–212.
- [5] T. CHAN AND S. ESEDOGLU, *Aspects of total variation regularized l^1 function approximation*, SIAM Journal on Applied Mathematics, 65 (2005), pp. 1817–1837.
- [6] T. CHAN AND P. MULET, *On the convergence of the lagged diffusivity fixed point method in total variation image restoration*, SIAM Journal on Numerical Analysis, 36 (1999), pp. 354–367.
- [7] D. COLTUC AND P. BOLON, *Exact histogram specification*, IEEE Transactions on Image Processing, 15 (2006), pp. 1143–1152.
- [8] D. GEMAN AND G. REYNOLDS, *Constrained restoration and recovery of discontinuities*, IEEE Transactions on Pattern Analysis and Machine Intelligence, PAMI-14 (1992), pp. 367–383.
- [9] S. MALLAT, *A Wavelet Tour of Signal Processing*, Academic Press, San Diego, 2009.
- [10] M. NIKOLOVA, *Analytical bounds on the minimizers of least squares*, Inverse Problems in Imaging 1(4) (2007), pp. 661–677.
- [11] M. NIKOLOVA, Y.-W. WEN, AND R. CHAN, *Exact histogram specification for digital images using a variational approach*, Journal of Mathematical Imaging and Vision, online November 2012.

- [12] Y. WAN AND D. SHI, *Joint exact histogram specification and image enhancement through the wavelet transform*, IEEE Transactions on Image Processing, 16 (2007), pp. 2245–2250.
- [13] E. WEISZFELD, *Sur le point pour lequel la somme des distances de n points donnés est minimum*, Tôhoku Mathematics Journal 43 (1937), pp. 355–386.

Addresses:

F. Baus
Fraunhofer ITWM
Fraunhofer Platz 1
67663 Kaiserslautern
Germany

M. Nikolova
CMLA, ENS Cachan CNRS
61 av. du President Wilson
94235 Cachan Cedex
France
`nikolova@cmla.ens-cachan.fr`

G. Steidl
University of Kaiserslautern
Department of Mathematics
Paul-Ehrlich-Str. 31
67663 Kaiserslautern
Germany
`steidl@mathematik.uni-kl.de`

The work of M. Nikolova was supported in part by the "FMJH Program Gaspard Monge in optimization and operation research", and by the support to this program from EDF.